Materials Science Forum Vol. 651 (2010) pp 79-95

doi:10.4028/www.scientific.net/MSF.651.79

Direct access to the order parameter: parameterized symmetry modes and rigid body movements as a function of temperature

MÜLLER Melanie[1,a], DINNEBIER Robert E[1,b]., ALI Naveed Z.[1,c], CAMPBELL Branton J.[2,d] and JANSEN Martin[1,e]

[1]Max Planck Institute for Solid State Research, Heisenbergstr.1, 70569 Stuttgart, Germany

[2] Department of Physics & Astronomy, Brigham Young University, N261 ESC, BYU, Provo, UT 84602

[a]m.mueller@fkf.mpg.de, [b]r.dinnebier@fkf.mpg.de, [c]n.ali@fkf.mpg.de,

[d]branton_campbell@byu.edu, [e]m.jansen@fkf.mpg.de

Keywords: $CsFeO_2$, structural phase transition, symmetry-mode analysis, order parameter, spontaneous strain, critical exponent, rigid bodies, parametric Rietveld refinement.

Abstract

The first order phase transition of $CsFeO_2$ was investigated using synchrotron powder diffraction data as a function of temperature. Two alternative approaches were used to describe the deviation of the framework crystal structure relative to the high-symmetry parent structure: symmetry (a.k.a. distortion) modes and polyhedral-tilt parameters. In both cases, the relevant parameters were refined as a function of temperature using the method of parametric Rietveld refinement. We demonstrate a semi-automated and generally applicable method for the determination of spontaneous lattice strain variations, order parameters and power-law exponents as derived from Landau theory.

Introduction

Many crystalline phases can be viewed as low-symmetry distortions of real or hypothetical higher-symmetry parent structures (i.e. aristotypes). In such cases, a group-subgroup relationship must exist between the two structures, so that all symmetry elements of the low-symmetry phase are also present in the high symmetry phase. The low-symmetry phase will generally have more structural degrees of freedom than the parent phase, and may involve some combination of magnetic, displacive, occupancy and strain degrees of freedom. Using group-representation theory, these degrees of freedom can always be parameterized in terms of basis functions of the irreducible representations (irreps) of the parent symmetry, which we refer to as symmetry-adapted distortion modes, or more simply as symmetry-modes. The symmetry modes of a given type (e.g. lattice strain, displacive, occupancy or magnetic) belonging to the same irrep collectively comprise an "order parameter". The key order parameters that define a structural transition have zero amplitude on the high-symmetry side, and take on non-zero amplitudes on the low-symmetry side. These order parameters tend to place the daughter atoms of a given parent atom onto more general Wyckoff sites and often split a parent atom across multiple unique daughter sites. In many cases, the symmetry-adapted description is the most natural parameter set, because nature's order parameters are usually selected to break a specific set of symmetries.

In case of framework crystal structures, whose structural distortions involve rigid polyhedral units, the most natural description comprise tilt modes that leave the polyhedra undistorted [1, 2]. To account for this additional chemical information, one uses rotations, translations, and torsions as adjustable parameters. If the voids of the framework are occupied by guest atoms or molecules, these entities may also translate and/or reorient. The rigid-body (RB) description is more restrictive

than the symmetry-mode (SM) basis, which is helpful when only RB behavior is observed. But a single symmetry-adapted order parameter will often approximate a rigid-body mode for small mode amplitudes; and a linear combination of symmetry modes can achieve any possible distortion, including RB distortions.

If the distorted structure has a lower point group symmetry than the parent structure, the distortion can be referred to as ferroic. A ferroic distortion can be further classified as ferroelastic if it changes the shape of the unit cell in such a way as to alter the crystal system. A ferroelastic distortion can be described in terms of spontaneous macroscopic strains (ε_s) of the parent unit cell parameters. The ferroelastic transition then marks the boundary between the low-symmetry ferroelastic phase and a higher-symmetry paraelastic phase that supports only disordered local strains. Landau theory describes the main physical features of most ferroelastic phase transitions, wherein the thermodynamic state of the system and the free-energy difference that stabilizes the low-symmetry phase (the excess Gibbs free energy) are expressed in terms of thermodynamic order parameters [3,4]. Here, we will treat the lattice strains as linear combinations of symmetry-adapted gamma-point order parameters, which may also be coupled to additional displacive order parameters.

In Landau theory, an order parameter decreases continuously to zero at a second-order (a.k.a. continuous) phase transition, whereas an order parameter can abruptly "jump" to a non-zero value at a first-order (a.k.a. hysteretic) transition. For a continuous transition, the order parameter's dependence on temperature can be modeled by an empirical power law of the form

$$Q = f\,|T_{crit} - T|^{\beta}, \qquad (1)$$

where T_{crit} is the transition temperature, β is the critical exponent, and f is a temperature coefficient. Typical values of β are ½ for ordinary scalar second-order transitions, or ¼ for a transition at the tricritical point that marks the boundary between first and second-order transitions. Values between ¼ and ½ might be obtained for a variety of reasons [5,6]. The Landau critical exponent is derived by calculating the first derivative of the power series expansion of a truncated Gibbs free energy with respect to the order parameter and setting it to zero, a simplistic approach that is really only valid in a small temperature interval around T_{crit}. However, it has also been shown that non-standard power-law exponents obtained from fits over extended temperature ranges are often due to temperature-dependent energy-expansion coefficients of order four or higher and have nothing at all to do with critical phenomena [7,8]. And finally, attempting to fit a power-law to an order parameter that is only approximately second order, will artificially suppress the exponent due to the unusually rapid descent near the transition.

The most common method of characterizing structural phase transitions is powder x-ray or neutron diffraction. Modern lab instruments and advanced scattering facilities now provide for the rapid collection of high resolution powder diffraction patterns as a function of parameters like temperature, pressure or simple time. 1D or 2D position sensitive detectors allow for efficient measurements of a series of powder pattern near a phase transition. Usually, powder diffraction patterns are refined individually, followed by a post-refinement analysis of lattice parameters or atomic coordinates as a function of external variables. But with the availability of flexible self-programmable Rietveld programs like TOPAS, the simultaneous refinement of a single parametric model against multiple datasets has now become possible [9]. User-friendly software packages that allow one to automatically reparameterize a low-symmetry structure in terms of symmetry-adapted order parameters of a higher symmetry structure have also become available (e.g. ISODISPLACE [10, 11] and AMPLIMODES [12]), and require only a very basic knowledge of group theory. Together, these developments have enabled fast and stable parametric refinements of physically-meaningful order parameters that were previously impractical.

In this paper, the ferroelastic phase transition of $CsFeO_2$ is investigated in detail via parametric Rietveld refinement as a function of temperature. Both displacive and strain order parameters are modeled using power-law trends below T_{crit}. The displacive order parameters are analyzed using both the RB and SM descriptions for comparison purposes.

Method

Both RB and SM distortion models have been used to study the ferroelastic phase transition of $CsFeO_2$ from a cubic (space group $Fd\bar{3}m$) parent structure to an orthorhombic (space group *Pbca*) low-symmetry structure (Fig. 2). We describe the SM approach first. Starting with $Fd\bar{3}m$ and *Pbcn* CIF-structure files that were derived from single-crystal x-ray diffraction data from isotypic $RbFeO_2$ [13], the ISODISPLACE software was used to perform an automatic symmetry-mode decomposition of the low-symmetry distorted structure into modes of the high-symmetry cubic parent. In the cubic phase, despite having a total of 32 atoms in the conventional face-centered unit cell, the structure of CsFeO2 has no free atomic coordinates. The cubic cell contains one unique atom of each type, each of which lies on a special Wyckoff point. In the orthorhombic phase, however, there are 24 free atomic coordinates. Because the symmetry-mode basis is related to the traditional atomic-coordinate basis by a linear transformation, there must also be 24 displacive symmetry modes, which are listed in Table 1.

Each mode in Table 1 has rather long name that includes the parent space-group symmetry to which the mode belongs, the k-point (i.e. the point in reciprocal space that will get intensity if the mode is activated), the space-group irrep label and order parameter direction (dictates which space-group symmetry operations are preserved by the mode), the parent atom affected by the mode and its Wyckoff site, the irrep of the point-group symmetry (dictates which site symmetry operations are preserved by the mode) and the order parameter branch [10]. For convenience, we number these modes from 1 to 24. Note that we use Miller-Love notation for all irrep labels. Eq. 2 shows how the atomic positions $\mathbf{r}_j$ of the low-symmetry (LS) and high-symmetry (HS) phases are related [1].

$$\mathbf{r}_j^{LS} = \mathbf{r}_j^{HS} + \sum_m c_{j,m} Q_m \boldsymbol{\varepsilon}(j|m) \qquad (2)$$

The *j* index indicates an atom in the low-symmetry supercell, the *m* index runs over all of the modes associated with its parent atom, $\boldsymbol{\varepsilon}(j|m)$ is the j^{th} component of the unnormalized polarization vector of the m^{th} mode, and the $c_{j,m}$ are normalization coefficients such that $\sum_j c_{j,m}^2 \boldsymbol{\varepsilon}(j|m)^2 = 1$. Q_m is the amplitude of the m^{th} mode, and equals the root-summed-squared displacement, summed over all supercell atoms affected by the mode. ISODISPLACE essentially used group-theoretical methods to compute the symmetry-mode polarization vectors and normalization coefficients, and then saved the results as a system of linear equations in TOPAS .str format [11].

Table 1: Symmetry-adapted distortion modes available to the ferroelastic phase transition of $CsFeO_2$ from *Fd-3m* to *Pbca* symmetry. The ten modes that were actually used for parametric Rietveld refinements appear in bold.

	name	description of mode
1	a1	Fd-3m[0,0,0]GM5+(a,0,0)[cs:b]T2
2	**a2**	**Fd-3m[0,3/2,0]DT5(0,0,0,0,0,0,0,0,a,-2.414a,2.414a,a)[cs:b]T2_1(a)**
3	a3	Fd-3m[0,3/2,0]DT5(0,0,0,0,0,0,0,0,a,-2.414a,2.414a,a)[cs:b]T2_2(a)
4	**a4**	**Fd-3m[1/2,1/2,0]SM2(0,a,0,0,0,0,0,0,0,0,0,0)[cs:b]T2(a)**
5	a5	Fd-3m[1/2,1/2,1/2]L3+(0,0,0,0,a,-a,-a,a)[cs:b]T2(a)
6	a6	Fd-3m[0,1,0]X1(0,a,0,0,0,0)[cs:b]T2(a)
7	a7	Fd-3m[0,0,0]GM5+(a,0,0)[Fe:a]T2(a)
8	a8	Fd-3m[0,3/2,0]DT5(0,0,0,0,0,0,0,0,a,-2.414a,2.414a,a)[Fe:a]T2_1(a)
9	**a9**	**Fd-3m[0,3/2,0]DT5(0,0,0,0,0,0,0,0,a,-2.414a,2.414a,a)[Fe:a]T2_2(a)**
10	**a10**	**Fd-3m[1/2,1/2,0]SM2(0,a,0,0,0,0,0,0,0,0,0,0)[Fe:a]T2(a)**
11	a11	Fd-3m[1/2,1/2,1/2]L3+(0,0,0,0,a,-a,-a,a)[Fe:a]T2(a)
12	a12	Fd-3m[0,1,0]X1(0,a,0,0,0,0)[Fe:a]T2(a)
13	a13	Fd-3m[0,3/2,0]DT5(0,0,0,0,0,0,0,0,a,-2.414a,2.414a,a)[O:c]A2u(a)
14	**a14**	**Fd-3m[0,3/2,0]DT5(0,0,0,0,0,0,0,0,a,-2.414a,2.414a,a)[O:c]Eu_1(a)**
15	**a15**	**Fd-3m[0,3/2,0]DT5(0,0,0,0,0,0,0,0,a,-2.414a,2.414a,a)[O:c]Eu_2(a)**
16	**a16**	**Fd-3m[1/2,1/2,0]SM2(0,a,0,0,0,0,0,0,0,0,0,0)[O:c]A2u(a)**
17	**a17**	**Fd-3m[1/2,1/2,0]SM2(0,a,0,0,0,0,0,0,0,0,0,0)[O:c]Eu_1(a)**
18	**a18**	**Fd-3m[1/2,1/2,0]SM2(0,a,0,0,0,0,0,0,0,0,0,0)[O:c]Eu_2(a)**
19	**a19**	**Fd-3m[1/2,1/2,1/2]L2+(0,0,a,-a)[O:c]Eu(a)**
20	a20	Fd-3m[1/2,1/2,1/2]L3+(0,0,0,0,a,-a,-a,a)[O:c]A2u(a)
21	a21	Fd-3m[1/2,1/2,1/2]L3+(0,0,0,0,a,-a,-a,a)[O:c]Eu_1(a)
22	a22	Fd-3m[1/2,1/2,1/2]L3+(0,0,0,0,a,-a,-a,a)[O:c]Eu_2(a)
23	a23	Fd-3m[0,1,0]X1(0,a,0,0,0,0)[O:c]A2u(a)
24	a24	Fd-3m[0,1,0]X1(0,a,0,0,0,0)[O:c]Eu(a)

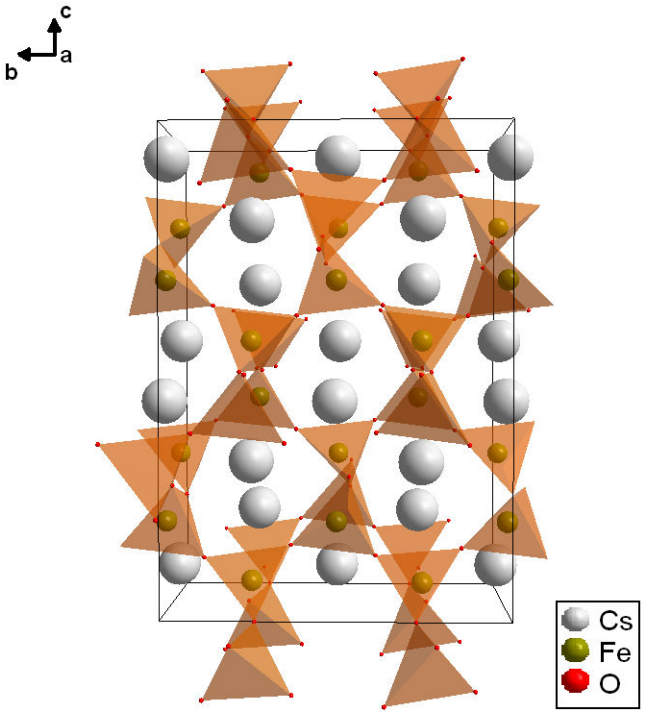

Fig. 2: An *a*-axis projection of the low-temperature (*Pbca*) crystal structure of $CsFeO_2$.

Ten of the 24 displacive symmetry modes were identified as being necessary to describe the phase transition: two (*a*2 and *a*4) for caesium, two (*a*9 and *a*10) for iron and six (*a*14, *a*15, *a*16, *a*17, *a*18 and *a*19) for oxygen. The *a*2-mode affects the *y*-coordinates of both Cs atoms, while *a*4 only affects the *x*-coordinate of Cs2. The *a*10 mode influences the *y*-coordinate of the Fe1 and Fe2 atoms while the *a*10 mode influences only the *x*-coordinate of the Fe1 atom. Oxygen modes *a*14 to *a*19 cooperate to describe the rotation of the FeO_4 tetrahedron, which should not be substantially distorted. The involved modes were classified considering different properties: modes with small amplitudes were assumed to be not important as they cause only minimal changes of atomic positions. ISODISPLACE [10] was used to control the shift of the atoms. To assure that no important mode was neglected, it was checked that additional modes do not lead to a better fit.

Next, we describe implementation of the rigid-body model, in which the low-symmetry distortion was defined in terms of polyhedral tilt angles [2] that left the polyhedra themselves undistorted. A suitable rigid building unit that describes both the low and high-temperature $CsFeO_2$ structures consists of two regular corner-sharing FeO_4 tetrahedra that are tilted with respect to each other as shown in Fig. 3. Taking symmetry equivalent positions into account, the resulting rigid body consists of four oxygen and two iron atoms with two tilting angles and the average Fe-O distance as internal degrees of freedom, as illustrated in Fig. 4. The two tilt angles are (1) the Fe1-O1-Fe2 (tilt-1) bond angle and (2) the O4-Fe2-O1-Fe1 tortion angle (tilt-2) between the two tetrahedra. For the Rietveld refinement, the rigid body was set up in form of a z-matrix (Table 2) that naturally describes the position of each atom in terms of its distance, angle and torsion angle relative to previously defined atoms [14]. The bridging O1 oxygen atom of the two tetrahedra was used as the centre of the rigid body. The orientation and position of the rigid body relative to the internal coordinate system of the crystal was found to be constant over the entire temperature range of investigation and thus only the three internal degrees of freedom were subjected to refinement. As the two Cs atoms in the voids of the framework are independent of the rigid body, their crystallographically relevant atomic coordinates were refined separately.

Table 2: Z-matrix description [14] of the crystallographically independent atoms of the Fe_2O_7 rigid body in *Pbca* symmetry. The three internal refinable parameters (tilt-1, tilt-2 and r) are displayed in bold.

Atom	Distance	angle	torsion angle	related atoms
O1	0			
Fe1	**r**			O1
O2	**r**	109.47		Fe1 O1
O3	**r**	109.47	120	Fe1 O2 O1
Fe2	**r**	**tilt-1**	180	O1 Fe1 O2
O4	**r**	109.47	**tilt-2**	Fe2 O1 O2

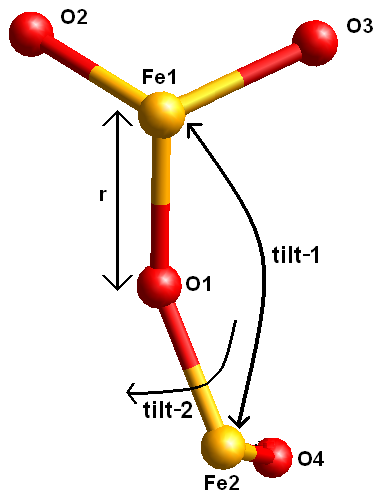

Fig. 3: Rigid body consisting of the crystallographically independent atoms of the structure building double tetrahedron in $CsFeO_2$ exhibiting three internal parameters: r, tilt-1 and tilt-2.

The technique of parametric Rietveld refinement [9] was applied to both the SM and RB models. This technique enables the refinement of various (e.g. thermodynamic) parameters directly from diffraction data. Prior to parametric refinement, preliminary refinements were performed at each temperature individually, and the temperature dependence of each candidate symmetry mode or z-matrix parameter was examined in order to identify the parameter subset that captures the principal features of the distortion. Then, for the parametric refinement, these crystallographic structural parameters were not refined directly, but were rather modeled as power-law temperature trends (Eq. 1), so that each one possessed a temperature-independent power-law exponent and coefficient [3]. Each z-matrix parameter in the RB model possessed an unique refinable coefficient and exponent. In the SM model, however, all modes belonging to a single order parameter (labeled according to irrep) shared the same power-law exponent. The temperature-independent power law exponents and coefficients were then subjected to parametric refinement, simultaneously against diffraction patterns collected at all temperatures. Topas (Version 4.1; Bruker AXS) was used to perform the refinements [15].

The characterization of the lattice strain below the ferroelastic phase transition is also important here. Strain is a symmetric second rank tensor that can be represented by a 3×3 matrix which for the orthorhombic symmetry (actual supercell) reduces to a diagonal matrix with the following diagonal elements:

$$e_{11s} = \frac{a_s}{a_{s0}} - 1 = \frac{a_s}{a_{p0}/\sqrt{2}} - 1$$
$$e_{22s} = \frac{b_s}{b_{s0}} - 1 = \frac{b_s}{\sqrt{2}a_{p0}} - 1 \quad , \qquad (3)$$
$$e_{33s} = \frac{c_s}{c_{s0}} = \frac{c_s}{2\,a_{p0}} - 1$$

with the lattice parameters of the supercell a_s, b_s., c_s and the isothermal lattice parameters a_{s0}, b_{s0} and c_{s0}. The isothermal lattice parameters a_{s0}, b_{s0} and c_{s0} can be also calculated from the isothermal lattice parameter of the cubic parent cell a_{p0}.

A more convenient way to set up these equations can be done in dependence on the cubic parent cell. In the high-symmetry cubic phase, the strain is a diagonal matrix such that

$$e_{11p} = e_{22p} = e_{33p} \quad \text{and} \quad e_{12p} = e_{23p} = e_{13p} = 0 . \tag{4}$$

Upon formation of the ferroelastic strain, the parent cell becomes a pseudo-cubic monoclinic cell defined by three independent order parameters that we will denote by ε_Γ, where Γ indicates one of three strain mode irreps: Γ_1^+, Γ_3^+ and Γ_5^+. The Γ_1^+ mode produces an isotropic volume expansion. The Γ_3^+ mode effects a tetragonal expansion of the parent *ab* plane and a compensating contraction of the *c* axis. The Γ_5^+ mode results in a monoclinic shear that changes the parent gamma angle and gives rise to a non-zero e_{12} strain component. In the coordinate system of the parent cell, the relationships between the lattice strains, the strain order parameters, the pseudo-cubic cell parameters (a_p, b_p, c_p, γ_p) and the unstrained cubic cell parameter, a_0, can be summed up as

$$\begin{aligned} e_{11p} &= e_{22p} = \varepsilon_{\Gamma_1^+} - \frac{1}{2}\varepsilon_{\Gamma_3^+} = \frac{a_p}{a_{p0}} - 1 = \frac{b_p}{a_{p0}} - 1 \\ e_{33p} &= \varepsilon_{\Gamma_1^+} + \varepsilon_{\Gamma_3^+} = \frac{c_p}{a_{p0}} - 1 \\ e_{12p} &= e_{21p} = \frac{1}{2}\varepsilon_{\Gamma_5^+} = \frac{\pi}{2} - \gamma_p \end{aligned} \tag{5}$$

The relationship between the strain of the supercell and the cubic strain is given in the following equation:

$$\begin{aligned} e_{11s} &= e_{11p} + e_{12p} \\ e_{22s} &= e_{11p} - e_{12p} \\ e_{33s} &= e_{33p} \end{aligned} \tag{6}$$

In the present parametric refinements, the supercell strain parameters were modeled as power-law trends vs. temperature. They are viewed as independent coupled order parameters and each possesses their own power-law exponents and coefficients (Eq. 7). In the parametric refinement, a conditional statement defined the region below the transition where the order parameters were permitted to have non-zero values.

$$\text{If } (T < T_{crit}) \text{ then } \varepsilon_\Gamma(T) = f_\Gamma (T_{crit} - T)^{\beta_\Gamma}, \text{ else } \varepsilon_\Gamma = 0 . \tag{7}$$

During parametric refinement the exponents and coefficients of the strain (Eq. 3) were used to calculate the supercell lattice parameters at each temperature.

It was necessary to treat the cubic parent cell parameter as a temperature-dependent quantity, a_0(T), and to linearly extrapolate it into the region of the low symmetry phase in order to correct for the additional effects of thermal expansion [16]. The slope (m_0) and intercept (t_0) used for this extrapolation were also part of the parametric refinement.

Experiment

Material

The sample was prepared using the azide/nitrate route [17, 18] from $CsNO_3$ (Sigma Aldrich, 99%), cesium azide (CsN_3) and active iron oxide (Fe_2O_3) according to the following equation:

$$5\ CsN_3 + CsNO_3 \rightarrow 6\ CsFeO_2 + 8\ N_2 \qquad (8)$$

The starting materials were mixed in the ratio required according to Eq. 19, ground thoroughly in an agate mortar, pressed into pellets (Ø = 6 mm) under 10^5 N, dried in vacuum (10^{-3} mbar) at 400 K for 12 h and placed under argon into a tightly closed steel vessel, provided with a silver inlay. In a flow of dry argon, the following temperature profile was applied for $CsFeO_2$: 298-533 K (100 Kh^{-1}); 533-653 K (5 K h^{-1}); 653-833 K (20 K h^{-1}). The reaction product was later cooled down slowly to 673 K (5 K h^{-1}) and then to room temperature at a rate of 100 K h^{-1}. The powder obtained is very sensitive to humid air and must be handled in an inert atmosphere.

Measurement

Powder diffraction measurements were performed at the Materials Sciences (MS-Powder) beamline of the Swiss Light Source using synchrotron radiation of wavelength 0.49701 Å using the Microstrip Detector Mythen-II. The sample was sealed in a Hilgenberg quartz-glass capillary with a diameter of 0.3 mm. The diffraction patterns were collected on heating the powder sample from 303-409 K with steps of 1 K using a STOE capillary furnace. The powder patterns were recorded for 40 seconds (4 scans of 10 seconds each) in the angular range from 3.0° – 53.38° 2θ.

Results and Discussion

The dependence of the crystal structure of $CsFeO_2$ on temperature in the temperature range from 303 K to 409 K was investigated by sequential and parametric Rietveld refinement. Both symmetry mode (SM) and rigid-body (RB) refinements were performed. Fig. 4 illustrates the result of a single-temperature refinement based on SM parameters at T = 328 K. Fig. 5 illustrates the results from a temperature-dependent parametric symmetry-mode refinement against all available data sets throughout the temperature range investigated. The parametric model produced diffraction patterns that agreed well with corresponding experimental patterns at each temperature, demonstrating the effectiveness of the parametric approach and the inclusion of an adequate structural-parameter set. Including additional parameters did not significantly improve the quality of the fit.

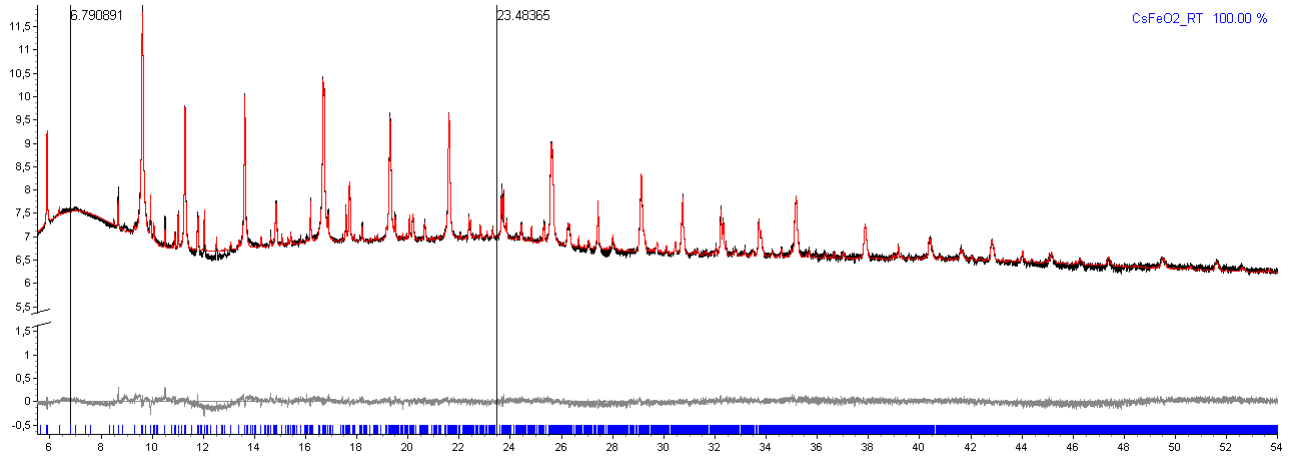

Fig. 4: Logarithmic plot of the single-point symmetry-mode refinement of $CsFeO_2$ at T = 328 K. The two peaks at 6.79° and 24.48° 2θ are used to model the background in addition to the Chebyshev polynomial.

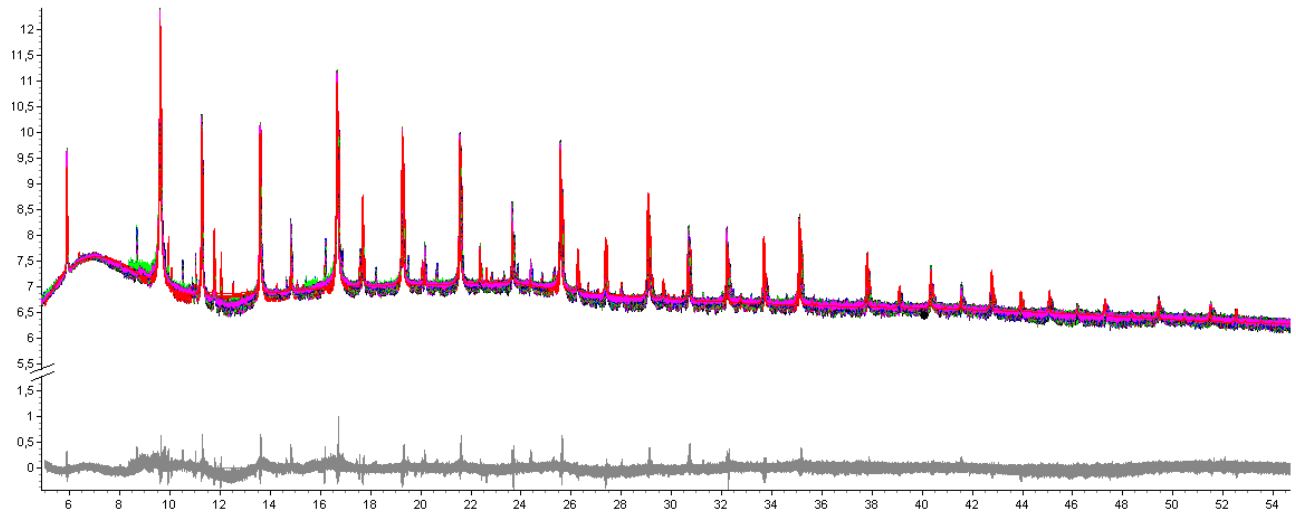

Fig. 5: Logarithmic plot of temperature-dependent parametric symmetry-mode refinement of $CsFeO_2$ in the temperature ranges from 303 K to 409 K. Observed, calculated and difference traces for all temperatures used (1 K steps) are shown in a stacked arrangement.

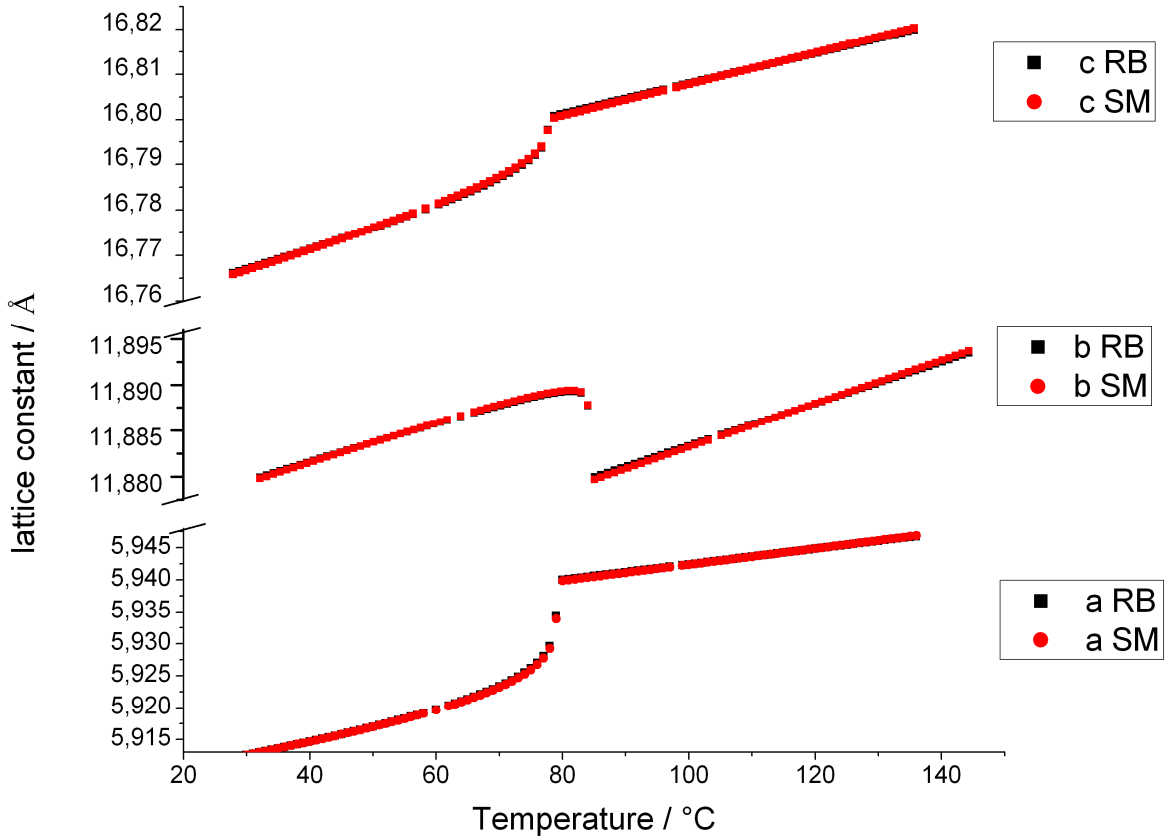

Fig. 6: Temperature-dependent supercell parameters for $CsFeO_2$ as calculated from parametrically-refined power-law models of the strain parameters.

For both types of parametric Rietveld refinements (SM, RB) (Fig. 5), the lattice parameters varied only slightly (Fig. 6). Below the phase transition, all strain order parameters (Fig. 7) and lattice parameters exhibit the anticipated power law trends, while above the transition, the lattice parameters can be adequately fitted using a linear function within the investigated temperature

range. The strain order parameters exhibited essentially the same development when applied to the SM and RB models. Observe that the magnitude of the strain component e_{11} is significantly higher than the magnitudes of e_{22} and e_{33}, which are of comparable size.

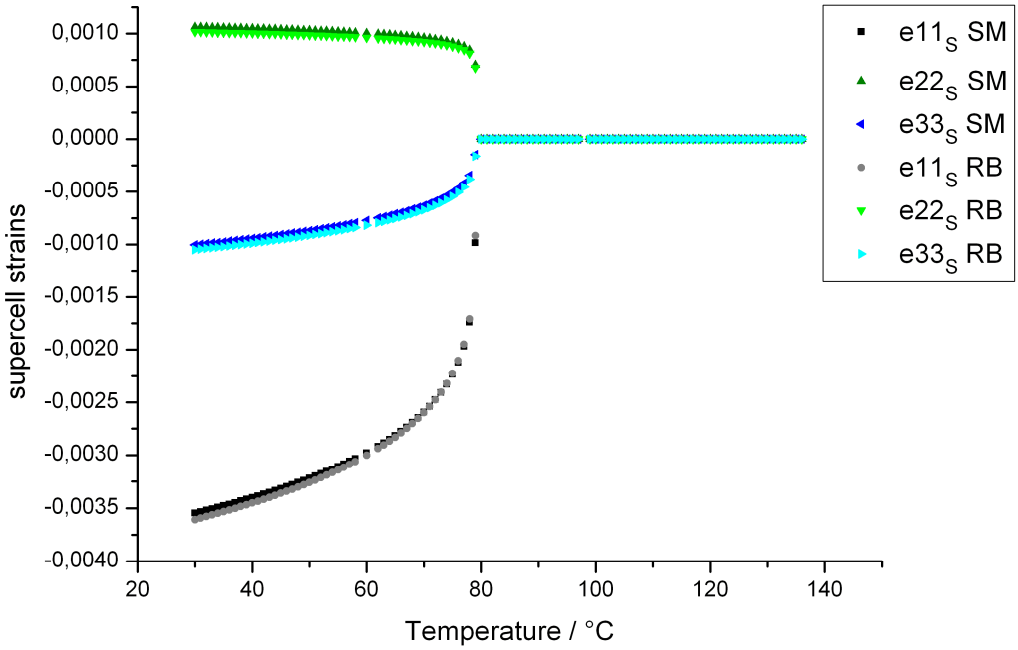

Fig. 7: Temperature-dependent supercell strains for $CsFeO_2$ as calculated from their parametrically-refined power-law models.

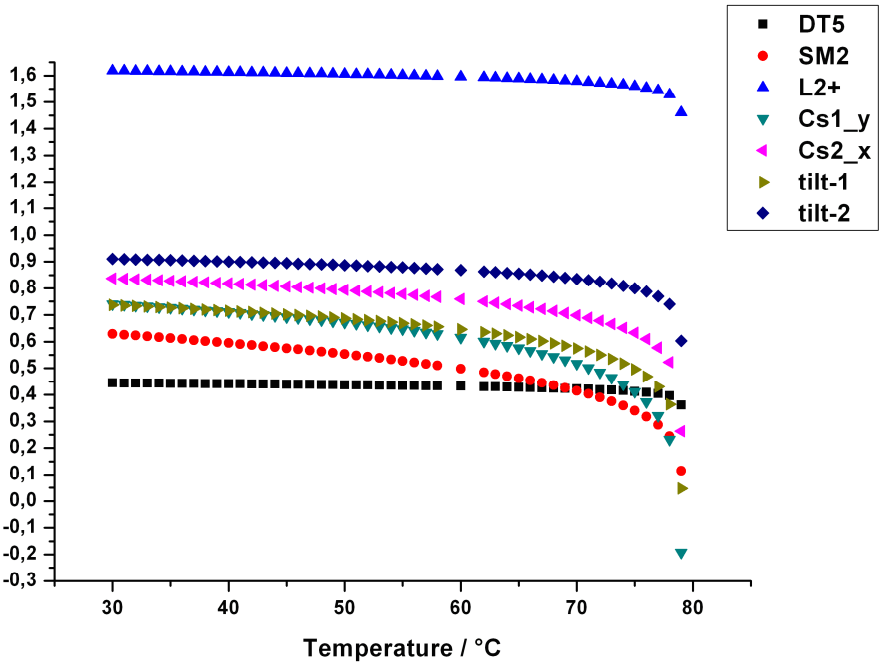

Fig. 8: Comparison of the root squared sum of the DT5, SM2 and L2+ with the normalised internal RB parameters in dependence on temperature. Temperature-dependent symmetry-mode amplitudes for $CsFeO_2$ as determined from their parametrically-refined power-law models.

The temperature-dependencies of the displacive degrees of freedom are plotted in Figure 8. These power-law curves were calculated using the parametrically-refined coefficients and exponents. The refined power-law coefficients and exponents are listed in Table 3. Note that the SM and RB refinements were performed separately, though their results are shown together.

If one views the set of all possible distortions possessing the requisite supercell and *Pbca* symmetry as a multi-parameter vector space, the traditional atomic-coordinate (TAC) and SM descriptions both span the entire distortion space. In contrast, the RB description is much more restrictive because it only allows distortions that preserve the shapes of the rigid polyhedra. Thus the RB description has far fewer free parameters. While the SM description has just as much freedom as the TAC description, only a relatively small fraction of the available symmetry modes tend to be important to a specific phase transition. And in the case of $CsFeO_2$, a relatively small number of symmetry modes can approximately reproduce the rigid-body motions observed.

Ideally, we would expect all of the modes associated with a single symmetry-adapted order parameter to evolve together, sharing the same power-law exponent, and we have assumed this to be the case in defining the SM model of $CsFeO_2$. The key displacive order parameters that contribute to the low-temperature $CsFeO_2$ distortion appear to be DT5 (Δ_5), SM2(Σ_2) and L2+(L_2^+). ISODISPLACE was used to determine that any two of these could comprise a potentially primary (i.e. capable of producing the symmetry of the distorted phase) pair of coupled order parameters. In general, coupled order parameters can arise at different temperatures and follow different trends. Or they can be strongly coupled, arising at nearly the same temperature and following very similar trends. Because sequential single-temperature refinements indicate that each of the important order parameters of $CsFeO_2$ arise within a 1 K temperature range, we assumed they all appear at the same temperature (352 K).

Because the DT5, SM2 and L2+ order parameters must cooperate in order to preserve the shapes of the FeO_4 tetrahedra, we can reasonably assume that they are strongly coupled by physical bonding constraints. Thus, we might expect them to exhibit similar temperature evolutions. The *a*15 and *a*19 symmetry modes, for example, must cooperate to mimic the RB tilt-2 angle, and therefore are coupled with the same power-law exponents. Because the SM and RB models are roughly equivalent, it is not surprising that the DT5/L2+ power-law exponent is similar to that of the RB tilt-2 angle itself. Other relationships between the two models include the *a*10 symmetry mode, which approximates the RB tilt-1 angle, and the *a*2 and *a*4 symmetry modes which are related to the Cs positions of the RB model. In each of these cases, the power-law exponents of geometrically-related SM and RB parameters are very similar as expected.

The small values obtained for the power-law exponents in Table 3 should not be overinterpreted. They are, most likely, a result of the fact that this phase transition is actually first order. Based on Landau and renormalization-group theory considerations, ISODISPLACE determined that none of the DT5, SM2 or L2+ order parameters of the $CsFeO_2$ distortion are capable of producing continuous transitions when acting alone, and certainly not when acting simultaneously. Though the transition appears to be approximately second order in nature, first-order distortions that evolve too quickly below the transition do provide a simple explanation for the unusually-small power-law exponents that we observe.

Table 3: Comparison of effective power-law coefficients and exponents obtained from parametric Rietveld refinement of $CsFeO_2$ in dependence on temperature using two different methods.

symmetry mode	P.L. coeff.	P.L. exponent	rigid body	P.L. coeff.	P.L. exponent
a2(Δ_5)	0.066(1)	0.015(1)	Cs1*y*		0.26(1)
a4(Σ_2)	0.355(1)	0.123(2)	Cs2*x*		0.11(1)
a9(Δ_5)	0.145(3)	0.015(1)	tilt-1		0.168(2)
a10(Σ_2)	0.241(1)	0.123(2)	tilt-2		0.056(1)
a14(Δ_5)	0.622(12)	0.015(1)			
a15(Δ_5)	0.616(13)	0.015(1)			
a16(Σ_2)	0.213(4)	0.123(2)			
a17(Σ_2)	-0.061(5)	0.123(2)			
a18(Σ_2)	-0.499(5)	0.123(2)			
a19(L_2^+)	1.528(8)	0.015(1)			
ε_{11s}	-0.00172	0.185(1)	ε_{11s}	-0.0017	0.194(1)
ε_{22s}	0.00084	0.059(1)	ε_{22s}	0.00081	0.058(1)
ε_{33s}	-0.00034	0.277(2)	ε_{33s}	-0.00038	0.262(2)

Conclusions

We have demonstrated the semiautomated parametric refinement of structural order parameters that arise at the cubic-orthorhombic structural phase transition of $CsFeO_2$. This parametric refinement against diffraction patterns collected over a wide range of temperatures yielded power-law exponents and coefficients describing the evolution of the atomic displacements and the ferroelastic lattice-strains that contribute to the distortion. Two different parameterizations of the distortion, the symmetry-adapted distortion mode description and the internal rigid-body (i.e. z-matrix) description, proved to be closely related due to the natural tendency of symmetry modes to produce polyhedral tilts like those observed in $CsFeO_2$. With both models, the automated parametric refinement greatly increased the speed of the refinement and post-refinement analysis. To characterize power-law trends in structural order parameters, it was crucial to collect diffraction patterns at a sufficient number points above and below the phase transition, which is routinely possible at modern synchrotron sources. In the case of the present work, the interpretation of the power-law exponents was difficult due to fact that this structural phase transition is weakly first order. Yet, the parametric Rietveld refinement of symmetry modes and internal rigid body parameters as a function of external variables proved to be a powerful tool for investigating structural phase transitions. The principle benefit lies in the flexibility and convenience of identifying, testing and comparing candidate order parameters. The development of third party software for further automation of this rather complicated process is under way.

References:

[1] R.J. Angel, N.L. Ross and J. Zhao: Eur. J. Mineral. 17 (2005), p. 193

[2] R.M. Hazen and L.W. Finger: Comparative Crystal Chemistry (John Wiley and Sons, 1982)

[3] E.K.H. Salje: Phase transitions in ferroelastic and co-elastic crystals (Cambridge University press, 1990)

[4] E.K.H. Salje: Acta Cryst. A47 (1991), p. 453

[5] J.F. Scott, S.A. Hayward and M. Miyake: J. Phys.: Condens. Matter 17 (2005), p. 5911

[6] M.C. Gallardo, F. J. Romero, S. A. Harward, E.K.H. Salje and J. del Cerro: Miner. Mag. 64 (2000), p. 971

[7] A.P. Giddy, M.T. Dove and V. Heine: J. Phys.: Condens. Matter 1 (1989), p. 8327

[8] S. Radescu, I. Etxebarria and J.M. Pérez-Mato: J. Phys.: Condens. Matter 7 (1995), p.585

[9] G.W Stinton and J.S.O. Evans: J. Appl. Cryst. 40 (2007), p. 87

[10] B.J. Campbell, H.T. Stokes, D.E. Tanner and D.M. Hatch: J. Appl. Cryst. 39 (2006), p. 607

[11] B.J. Campbell, J S.O. Evans, F.Perselli, H.T.Stokes, IUCr Computing Commission Newsletter 8, 81-95 (2007)

[12] D. Orobengoa, C. Capillas, M.I. Aroyo and J.M. Perez- Mato: J. Appl. Cryst. A42 (2009), p. 820

[13] J. Nuss, N. Z. Ali, M. Jansen: Acta Crys. B63 (2007), p. 719

[14] A.R. Leach: Molecular Modelling: Principles and Applications (Prentice-Hall, 1996)

[15] Topas, V. 4.1; Bruker AXS

[16] M.A. Carpenter, E.K.H. Salje and A. Graeme-Barber: Eur. J. Mineral. 10 (1998), p. 621

[17] D. Trinschek and M. Jansen: Angew. Chem. 111 (1999), p. 234

D. Trinschek and M. Jansen: Angew. Chem. Int. Ed. Engl. 38 (1999), p. 133

[18] M. Sofin, E.-M. Peters and M. Jansen: Z. Anorg. Allg. Chem. 628 (2002), p. 2697

Appendix:

Topas script for the parameterized distortion modes of $CsFeO_2$ in dependence on temperature

```
do_errors
conserve_memory

r_wp  6.826 r_exp  3.022 r_p  5.131 r_wp_dash  10.355 r_p_dash  10.644 r_exp_dash  4.584
weighted_Durbin_Watson  44.981 gof  2.259

'Temperatures
prm !t_30 30
prm !t_31 31
…
list of all different temperatures
…
prm !t_135 135
prm !t_136 136

'temperature at end of transition
prm t_crit  79.04822_0.01099

'parameters of parametric functions
prm !f_a1 0
prm f_a2  0.06639`_0.00140
prm !f_a3  0
prm f_a4  0.35517`_0.00137
prm !f_a5 0
prm !f_a6 0
prm !f_a7 0
prm !f_a8 0
prm f_a9  0.14451`_0.00263
prm f_a10  0.24105`_0.00122
prm !f_a11 0
prm !f_a12 0
prm !f_a13 0
prm f_a14  0.62236`_0.01275
prm f_a15  0.61578`_0.01311
prm f_a16  0.21265`_0.00394
prm f_a17 -0.06097`_0.00471
prm f_a18 -0.49873`_0.00456
prm f_a19  1.52795`_0.00750
prm !f_a20 0
…
prm !f_a24 0

prm !c_a1 0
prm c_a2  0.01487`_0.00137
prm !c_a3  0
prm c_a4  0.12326`_0.00114
prm !c_a5 0
prm !c_a6 0
prm !c_a7 0
prm !c_a8 0
prm c_a9 =c_a2;
prm c_a10  =c_a4;
prm !c_a11 0
prm !c_a12 0
prm !c_a13 0
prm c_a14 =c_a2;
prm c_a15 =c_a2;
prm c_a16 =c_a4;
prm c_a17 =c_a4;
prm c_a18  =c_a4;
prm c_a19 =c_a2;
prm !c_a20 0
prm !c_a21 0
prm !c_a22 0
prm !c_a23 0
```

```
prm !c_a24 0

prm f_e22  0.00084`_0.00000
prm c_e22  0.05950`_0.00077

prm f_e11 -0.00172`_0.00000
prm c_e11  0.18530`_0.00035

prm f_e33 -0.00034`_0.00000
prm c_e33  0.27720`_0.00174


prm c_lp0  8.38604`_0.00001
prm m_lp0  0.00018`_0.00000

'information about data
macro information {
       start_X  5
       finish_X  62
       LP_Factor( 90)
       Zero_Error(, 0.00545)
       exclude  0  0
       Rp 217.5
       Rs 217.5
       Slit_Width( 0.1)
       lam
              ymin_on_ymax  0.0001
              la  1 lo  0.497015 lh  1e-006
       x_calculation_step 0.005
}
/*
here for each pattern which is refined the details of the refinement are listed:
an example is given for the pattern at 70°C.
The contributions of other patterns only differ in the naming of parameters.
*/


...

 xdd "ch_070.xye"

bkg  @  391.161639`_1.1606305  361.363748`_2.12143128 -493.797701`_1.81476721
328.032304`_1.39636055 -135.272781`_1.07147052  3.13766804`_1.01669772
46.0996839`_0.88239319 -49.7190967`_0.870149416
r_wp  5.530 r_exp  2.999 r_p  4.293 r_wp_dash  8.274 r_p_dash  8.651 r_exp_dash  4.486
weighted_Durbin_Watson  0.495 gof  1.844
information

       str
              CS_L( , 757.72414_26.62824)
              Strain_L( , 0.09294_0.00125)
              r_bragg  100
              phase_name "CsFeO2_RT"
              cell_mass  3532.004
              cell_volume  1182.06002`_0.00842986465
              weight_percent  99.206`_0.093
              scale @  3.94380415e-006`_8.29e-009
              space_group Pbca
              Phase_LAC_1_on_cm( 78.46976`_0.00056)
              Phase_Density_g_on_cm3( 4.96171`_0.00004)

prm lp0_70 = c_lp0 + m_lp0*t_70;
prm a0_70 = lp0_70 / (2^0.5);
prm e_11_70 = If(t_crit >= t_70 , f_e11*(t_crit - t_70)^c_e11,0);
prm a_70 = ((e_11_70+1)*a0_70);
prm b0_70 = lp0_70*(2^0.5);
prm e_22_70 = If(t_crit >= t_70 , f_e22*(t_crit - t_70)^c_e22,0);
prm b_70 = ((e_22_70+1)*b0_70);
prm c0_70 = lp0_70*2;
prm e_70_70 = If(t_crit >= t_70 , f_e33*(t_crit - t_70)^c_e33,0);
prm c_70 = ((e_70_70+1)*c0_70);
```

```
            a=a_70;
            b=b_70;
            c=c_70;

'mode definitions
        prm  a1_70  = If(t_crit >= t_70 , f_a1*(t_crit - t_70)^c_a1,0);
        prm  a2_70  = If(t_crit >= t_70 , f_a2*(t_crit - t_70)^c_a2,0);
        prm  a3_70  = If(t_crit >= t_70 , f_a3*(t_crit - t_70)^c_a3,0);
        prm  a4_70  = If(t_crit >= t_70 , f_a4*(t_crit - t_70)^c_a4,0);
        prm  a5_70  = If(t_crit >= t_70 , f_a5*(t_crit - t_70)^c_a5,0);
        prm  a6_70  = If(t_crit >= t_70 , f_a6*(t_crit - t_70)^c_a6,0);
        prm  a7_70  = If(t_crit >= t_70 , f_a7*(t_crit - t_70)^c_a7,0);
        prm  a8_70  = If(t_crit >= t_70 , f_a8*(t_crit - t_70)^c_a8,0);
        prm  a9_70  = If(t_crit >= t_70 , f_a9*(t_crit - t_70)^c_a9,0);
         prm  a10_70  = If(t_crit >= t_70 , f_a10*(t_crit - t_70)^c_a10,0);
        prm  a11_70  = If(t_crit >= t_70 , f_a11*(t_crit - t_70)^c_a11,0);
        prm  a12_70  = If(t_crit >= t_70 , f_a12*(t_crit - t_70)^c_a12,0);
        prm  a13_70  = If(t_crit >= t_70 , f_a13*(t_crit - t_70)^c_a13,0);
        prm  a14_70  = If(t_crit >= t_70 , f_a14*(t_crit - t_70)^c_a14,0);
        prm  a15_70  = If(t_crit >= t_70 , f_a15*(t_crit - t_70)^c_a15,0);
        prm  a16_70  = If(t_crit >= t_70 , f_a16*(t_crit - t_70)^c_a16,0);
        prm  a17_70  = If(t_crit >= t_70 , f_a17*(t_crit - t_70)^c_a17,0);
        prm  a18_70  = If(t_crit >= t_70 , f_a18*(t_crit - t_70)^c_a18,0);
        prm  a19_70  = If(t_crit >= t_70 , f_a19*(t_crit - t_70)^c_a19,0);
         prm  a20_70  = If(t_crit >= t_70 , f_a20*(t_crit - t_70)^c_a20,0);
        prm  a21_70  = If(t_crit >= t_70 , f_a21*(t_crit - t_70)^c_a21,0);
        prm  a22_70  = If(t_crit >= t_70 , f_a22*(t_crit - t_70)^c_a22,0);
        prm  a23_70  = If(t_crit >= t_70 , f_a23*(t_crit - t_70)^c_a23,0);
        prm  a24_70  = If(t_crit >= t_70 , f_a24*(t_crit - t_70)^c_a24,0);

'mode-amplitude to delta-coord
       prm  Cs1_dx_70 = +  0.06089*a5_70;:  0.00000
       prm  Cs1_dy_70 = -  0.01165*a2_70 +  0.02813*a3_70;: -0.00080`_0.00002
       prm  Cs1_dz_70 = -  0.01522*a1_70 -  0.01522*a6_70;: -0.00000
       prm  Cs2_dx_70 = -  0.06089*a4_70;: -0.02837`_0.00013
       prm  Cs2_dy_70 = +  0.02813*a2_70 +  0.01165*a3_70;:  0.00193`_0.00004
       prm  Cs2_dz_70 = -  0.01522*a1_70 +  0.01522*a6_70;:  0.00000
       prm  Fe1_dx_70 = -  0.06089*a11_70;: -0.00000
       prm  Fe1_dy_70 = +  0.01165*a8_70 +  0.02813*a9_70;:  0.00420`_0.00008
       prm  Fe1_dz_70 = -  0.01522*a7_70 +  0.01522*a12_70;:  0.00000
       prm  Fe2_dx_70 = -  0.06089*a10_70;: -0.01926`_0.00011
       prm  Fe2_dy_70 = +  0.02813*a8_70 -  0.01165*a9_70;: -0.00174`_0.00003
       prm  Fe2_dz_70 = -  0.01522*a7_70 -  0.01522*a12_70;: -0.00000
       prm  O1_dx_70  = +  0.04306*a17_70 +  0.02486*a19_70 +  0.03515*a21_70 +
0.03189*a22_70;:  0.03581`_0.00035
       prm  O1_dy_70  = +  0.01758*a13_70 +  0.00725*a14_70 +  0.01209*a15_70 -
0.01758*a23_70 +  0.01243*a24_70;:  0.01235`_0.00019
       prm  O1_dz_70  = -  0.00879*a13_70 +  0.00725*a14_70 +  0.01209*a15_70 +
0.00879*a23_70 +  0.01243*a24_70;:  0.01235`_0.00019
       prm  O2_dx_70  = +  0.04306*a17_70 -  0.02486*a19_70 -  0.03515*a21_70 -
0.03189*a22_70;: -0.04269`_0.00035
       prm  O2_dy_70  = -  0.01758*a13_70 -  0.00725*a14_70 -  0.01209*a15_70 -
0.01758*a23_70 +  0.01243*a24_70;: -0.01235`_0.00019
       prm  O2_dz_70  = +  0.00879*a13_70 -  0.00725*a14_70 -  0.01209*a15_70 +
0.00879*a23_70 +  0.01243*a24_70;: -0.01235`_0.00019
       prm  O3_dx_70  = -  0.04972*a16_70 +  0.03515*a18_70;: -0.03687`_0.00034
       prm  O3_dy_70  = -  0.01243*a19_70 +  0.00879*a21_70 +  0.01907*a22_70;: -
0.01962`_0.00011
       prm  O3_dz_70  = -  0.01243*a16_70 -  0.01758*a18_70;:  0.00803`_0.00013
       prm  O4_dx_70  = -  0.02486*a19_70 -  0.04972*a20_70 +  0.01758*a21_70 +
0.00854*a22_70;: -0.03925`_0.00023
       prm  O4_dy_70  = +  0.02474*a14_70 +  0.00708*a15_70;:  0.02041`_0.00034
       prm  O4_dz_70  = -  0.01243*a19_70 +  0.01243*a20_70 +  0.00879*a21_70 +
0.00427*a22_70;: -0.01962`_0.00011

'distorted coordinates
        prm  Cs1_x_70 = 3/4 + Cs1_dx_70;:  0.75000
        prm  Cs1_y_70 = 0 + Cs1_dy_70;: -0.00080`_0.00002
        prm  Cs1_z_70 =    0.06250 + Cs1_dz_70;:  0.06250
        prm  Cs2_x_70 = 1/4 + Cs2_dx_70;:  0.22163`_0.00013
        prm  Cs2_y_70 = 1/4 + Cs2_dy_70;:  0.25193`_0.00004
```

```
        prm  Cs2_z_70 =    0.31250 + Cs2_dz_70;:  0.31250
        prm  Fe1_x_70 = 1/4 + Fe1_dx_70;:  0.25000
        prm  Fe1_y_70 = 0 + Fe1_dy_70;:  0.00420`_0.00008
        prm  Fe1_z_70 =    0.18750 + Fe1_dz_70;:  0.18750
        prm  Fe2_x_70 = 3/4 + Fe2_dx_70;:  0.73074`_0.00011
        prm  Fe2_y_70 = 1/4 + Fe2_dy_70;:  0.24826`_0.00003
        prm  Fe2_z_70 =    0.43750 + Fe2_dz_70;:  0.43750
        prm  O1_x_70  = 1/4 + O1_dx_70;:  0.28581`_0.00035
        prm  O1_y_70  = 1/8 + O1_dy_70;:  0.13735`_0.00019
        prm  O1_z_70  = 1/8 + O1_dz_70;:  0.13735`_0.00019
        prm  O2_x_70  = 1/4 + O2_dx_70;:  0.20731`_0.00035
        prm  O2_y_70  = 1/8 + O2_dy_70;:  0.11265`_0.00019
        prm  O2_z_70  = 5/8 + O2_dz_70;:  0.61265`_0.00019
        prm  O3_x_70  = 0 + O3_dx_70;: -0.03687`_0.00034
        prm  O3_y_70  = 1/4 + O3_dy_70;:  0.23038`_0.00011
        prm  O3_z_70  = 0 + O3_dz_70;:  0.00803`_0.00013
        prm  O4_x_70  = 1 + O4_dx_70;:  0.96075`_0.00023
        prm  O4_y_70  = 0 + O4_dy_70;:  0.02041`_0.00034
        prm  O4_z_70  = 1/4 + O4_dz_70;:  0.23038`_0.00011

                site Cs1 x = Cs1_x_70; y = Cs1_y_70; z = Cs1_z_70; occ Cs 1 beq @
2.2814`_0.0642
                site Cs2 x = Cs2_x_70; y = Cs2_y_70; z = Cs2_z_70; occ Cs 1 beq @
2.2764`_0.0693
                site Fe1 x = Fe1_x_70; y = Fe1_y_70; z = Fe1_z_70; occ Fe 1 beq @
0.8097`_0.1138
                site Fe2 x = Fe2_x_70; y = Fe2_y_70; z = Fe2_z_70; occ Fe 1 beq @
1.1939`_0.1268
                site O1  x = O1_x_70;  y = O1_y_70;  z = O1_z_70;  occ O  1 beq 1.0
                site O2  x = O2_x_70;  y = O2_y_70;  z = O2_z_70;  occ O  1 beq 1.0
                site O3  x = O3_x_70;  y = O3_y_70;  z = O3_z_70;  occ O  1 beq 1.0
                site O4  x = O4_x_70;  y = O4_y_70;  z = O4_z_70;  occ O  1 beq 1.0

      str
            CS_L( , 820.38984_26.94758)
            Strain_L( , 0.08747_0.00104)
            r_bragg  100
            phase_name "CsFeO2_HT"
            cell_mass  3532.004
            cell_volume  1179.21251`_0.360889842
            weight_percent  0.794`_0.093
            scale @  3.16261103e-008`_3.72e-009_LIMIT_MIN_1e-015
            space_group Pbca
            Phase_LAC_1_on_cm( 78.65924`_0.02407)
            Phase_Density_g_on_cm3( 4.97369`_0.00152)
            a  @  5.87288`_0.00082
            b  @  11.97029`_0.00182
            c  @  16.77398`_0.00379

        site Cs1 x = 0.75000;     y = 0;         z =0.06250;  occ Cs 1 beq 1
        site Cs2 x = 1/4;         y =1/4;        z = 0.31250; occ Cs 1 beq 1
        site Fe1 x = 1/4;         y = 0;         z = 0.18750; occ Fe 1 beq 1
        site Fe2 x = 3/4;         y = 1/4;       z = 0.43750; occ Fe 1 beq 1
        site O1  x = 1/4;         y = 1/8;       z = 1/8;     occ O  1 beq 1.0
        site O2  x = 1/4;         y = 1/8;       z = 5/8;     occ O  1 beq 1.0
        site O3  x = 0;           y = 1/4;       z = 0;       occ O  1 beq 1.0
        site O4  x = 1;           y = 0;         z = 1/4;     occ O  1 beq 1.0

xo_Is
            xo  6.79089064
            CS_L( ,0.56505)
            I   68.0074266
            peak_type fp
      xo_Is
            xo 23.4836519
            CS_L( ,0.98337)
            I   26.3336841
            peak_type fp
xdd "71.xye"
…
```